

OPEN ACCESS

Surface, Structural, and Electrochemical Analysis of High-Voltage Spinel Cathode $\text{LiNi}_{0.5}\text{Mn}_{1.5}\text{O}_4$ Evolution Upon Ambient Storage Conditions

To cite this article: Xuelian Liu *et al* 2023 *J. Electrochem. Soc.* **170** 100527

View the [article online](#) for updates and enhancements.

You may also like

- [Effect of Ti Substitution for Mn on the Structure of \$\text{LiNi}_{0.5}\text{Mn}_{1.5}\text{Ti}_x\text{O}_4\$ and Their Electrochemical Properties as Lithium Insertion Material](#)
J.-H. Kim, S.-T. Myung, C. S. Yoon *et al.*
- [Structural and Electrochemical Properties of \$\text{LiNi}_{0.5}\text{Mn}_{0.5}\text{O}_2\$ Thin-Film Electrodes Prepared by Pulsed Laser Deposition](#)
H. Xia, Y. S. Meng, M. O. Lai *et al.*
- [Thermal plasma synthesis and electrochemical properties of high-voltage \$\text{LiNi}_{0.5}\text{Mn}_{1.5}\text{O}_4\$ nanoparticles](#)
Hirotaka Sone, Shuhei Yoshida, Manabu Tanaka *et al.*



Your Lab in a Box!

The PAT-Tester-i-16: All you need for Battery Material Testing.

- ✓ All-in-One Solution with integrated Temperature Chamber!
- ✓ Cableless Connection for Battery Test Cells!
- ✓ Fully featured Multichannel Potentiostat / Galvanostat / EIS!







www.el-cell.com +49 40 79012-734 sales@el-cell.com

EL-CELL[®]
electrochemical test equipment





Surface, Structural, and Electrochemical Analysis of High-Voltage Spinel Cathode $\text{LiNi}_{0.5}\text{Mn}_{1.5}\text{O}_4$ Evolution Upon Ambient Storage Conditions

Xuelian Liu,¹ Marion Maffre,¹ Da Tie,¹  Nils Peter Wagner,²  Noelia Cortés Félix,³ Raheleh Azmi,⁴  Killian Stokes,^{2,4}  Per Erik Vullum,²  Jérôme Bailly,¹ Shubhadeep Pal,¹  Gary Evans,³ Mihaela Buga,⁵  Maria Hahlin,⁴  Kristina Edström,⁴  Simon Clark,²  and Alexandru Vlad^{1,z} 

¹Institute of Condensed Matter and Nanosciences, Université catholique de Louvain, Louvain-la-Neuve B-1348, Belgium

²SINTEF Industry, 7034 Trondheim, Norway

³Johnson Matthey, Technology Centre, Blounts Court, Sonning Common, RG4 9NH, United Kingdom

⁴Department of Chemistry—Ångström Laboratory, Uppsala University, 751 20 Uppsala, Sweden

⁵National Research and Development Institute for Cryogenic and Isotopic Technologies—ICSI, 240050 Ramnicu Valcea, Romania

Spinel $\text{LiNi}_{0.5}\text{Mn}_{1.5}\text{O}_4$ as one of the high-energy positive electrode materials for next generation Li-ion batteries has attracted significant interest due to its economic and environmental advantages. However, the sensitivity of this type of material upon short to long term ambient storage conditions and the impact on the electrochemical performances remains poorly explored. Nevertheless, this remains an important aspect for practical large-scale synthesis, storage and utilization. Herein, we study and compare the evolution of surface chemistry, bulk crystal structure and elemental content evolution and distribution of $\text{LiNi}_{0.5}\text{Mn}_{1.5}\text{O}_4$ using a variety of characterization techniques including XPS and STEM-EDS-EELS, as well as electrochemical analysis. We show that Mn species dominate the outer surface (0–5 nm), while Ni and Li are preferentially located further away and in the bulk. The studied $\text{LiNi}_{0.5}\text{Mn}_{1.5}\text{O}_4$ material is found to be stable, with minor changes in surface or bulk characteristics detected, even after 12 months of storage under ambient air conditions. The low surface reactivity to air also accounts for the minor changes to the electrochemical performance of the air-exposed $\text{LiNi}_{0.5}\text{Mn}_{1.5}\text{O}_4$, compared to the pristine material. This study provides guidance for the appropriate storage, handling and processing of this high-performance cathode material.

© 2023 The Author(s). Published on behalf of The Electrochemical Society by IOP Publishing Limited. This is an open access article distributed under the terms of the Creative Commons Attribution Non-Commercial No Derivatives 4.0 License (CC BY-NC-ND, <http://creativecommons.org/licenses/by-nc-nd/4.0/>), which permits non-commercial reuse, distribution, and reproduction in any medium, provided the original work is not changed in any way and is properly cited. For permission for commercial reuse, please email: permissions@iopublishing.org. [DOI: [10.1149/1945-7111/ad0263](https://doi.org/10.1149/1945-7111/ad0263)]



Manuscript submitted June 28, 2023; revised manuscript received September 13, 2023. Published October 23, 2023.

Supplementary material for this article is available [online](#)

Rechargeable lithium-ion batteries (LIBs) are ubiquitous in our modern lives, supplying electrical power to a wide range of applications, from small scale portable electronics to medium and large scale electric vehicles and residential storage units.^{1–4} To meet the ever-increasing demand for higher performance devices and vehicles, it is imperative to develop LIBs with higher energy densities and reduced environmental footprint.⁵ The use of spinel $\text{LiNi}_{0.5}\text{Mn}_{1.5}\text{O}_4$ (LNMO) materials as a positive electrode material is promising for next-generation high energy density LIBs.⁶ For instance, LNMO has a theoretical capacity of 147 mAh g^{-1} with high discharge voltage of ~ 4.7 V vs Li^+/Li , resulting in high energy content approaching 650 Wh kg^{-1} at the material level.⁷ Moreover, it has merits of high Li-ion diffusion and good thermal stability while applied as cathode material for LIBs.⁸ Other advantages include low cost and good sustainability metrics due to the absence of expensive and toxic cobalt.⁶

However, a series of challenges must be solved for LNMO to become a commercially competitive and massively applied cathode material. Typically, the LNMO-based cells suffer from capacity fade upon charge-discharge cycling mainly because of dissolution of transition metals, especially of Mn, into the electrolyte (leading primarily to SEI instability and corrosion at the anode), instability of electrode–electrolyte interphase, and electrolyte decomposition at high operating voltages of ~ 4.7 V vs Li^+/Li .^{9–11} Many strategies have been adopted to address these issues, often concerning the following aspects. First one is to protect the surface of the material by an engineered coating layer. For example, carbon coating is a very well established approach to not only stabilize the surface but also enhance the electronic conductivity of the cathodes.^{12,13} Other

coating materials, such as Li_3PO_4 , TiO_2 and polypyrrole for example, have been also shown to improve the electrochemical performance.^{14–16} The second strategy is correlated with electrolyte therapy via formulation optimization, use of additives and development of novel high-voltage electrolytes and additives.^{9,10,17} Doping is an additional simple and effective strategy to modify the intrinsic properties of electrode materials and in particular to boost Li ion diffusion and improve structural stability.^{18,19} LNMO materials doped with foreign cations (such as Na^+ , Mg^{2+} , Al^{3+} , Ti^{4+} for example) have shown improved cycling stability and rate capability.^{18,19}

Since the surface plays an important role in the electrochemical performance of LNMO cathode materials, surface analysis and evolution can be helpful to understand the electrochemical behavior upon aging.¹¹ For instance, ambient storage analyses is useful to determine how this material should be stored for long periods of time, or how the storage conditions can affect the surface structure and chemistry, and consequently, the electrochemical performances. For example, it has been reported that ambient conditions storage induces surface contamination species, resulting in degradation of the Ni-rich layered oxide cathodes including $\text{LiNi}_{0.8}\text{Co}_{0.1}\text{Mn}_{0.1}\text{O}_2$ (NCM811), $\text{LiNi}_{0.8}\text{Co}_{0.15}\text{Al}_{0.05}\text{O}_2$ (NCA) and $\text{LiNi}_{0.94}\text{Co}_{0.06}\text{O}_2$.^{20–24} While regeneration of the degraded cathode materials was found possible using thermal treatment, this represents an additional processing step, and could be difficult for manufacturers to realize this before cell production (in particular for coated electrodes).²⁰ It is worth noting that Mn-rich spinel oxides are considered to have good stability in ambient air (moisture and O_2 resistant), in comparison to Ni-rich layered oxides. For instance, surface coating with spinel $\text{LiMn}_{1.9}\text{Al}_{0.1}\text{O}_4$ has been, for example, reported to alleviate the chemical instability of Ni-rich $\text{LiNi}_{0.7}\text{Co}_{0.15}\text{Mn}_{0.15}\text{O}_2$ cathode material.²⁵ However, to the best of our knowledge, there is no

^zE-mail: alexandru.vlad@uclouvain.be

exhaustive investigation in literature on the ambient stability and storage aging of $\text{LiNi}_{0.5}\text{Mn}_{1.5}\text{O}_4$ materials.

In this work, an Al-doped $\text{LiNi}_{0.5}\text{Mn}_{1.5}\text{O}_4$ cathode material is investigated in terms of its susceptibility to long term ambient conditions storage. The $\text{LiNi}_{0.5}\text{Mn}_{1.5}\text{O}_4$ samples after different exposure durations (up to 12 months) have been analyzed and the electrochemical behavior compared. The results show minimal impact on the electrochemical response, indicating no significant degradation caused by ambient storage of this cathode material. For confirmation, various characterization techniques have been used to analyze and compare the pristine and exposed $\text{LiNi}_{0.5}\text{Mn}_{1.5}\text{O}_4$ including SEM, TEM-EELS, XPS, and electrochemical Li-storage. A comprehensive knowledge of the surface chemistry of the $\text{LiNi}_{0.5}\text{Mn}_{1.5}\text{O}_4$ is used to understand the influence of ambient storage on the electrochemical performance of the electrode and give guidance to storage and processing of this promising cathode material for practical applications.

Experimental

Sample preparation.—Al-doped $\text{LiNi}_{0.5}\text{Mn}_{1.5}\text{O}_4$ (with a nominal composition of $\text{Li}[\text{Ni}_{0.5}\text{Mn}_{1.45}\text{Al}_{0.05}]\text{O}_4$, hereafter noted as LNMO for simplicity) powder form material was supplied by Johnson Matthey. The as-received LNMO was split into different batches, stored for periods of 2 weeks (marked as LNMO_2w), 2 months (LNMO_2m), 6 months (LNMO_6m) and 12 months (LNMO_12m) while being continuously exposed to laboratory ambient air conditions. The storage was performed by placing the LNMO powder in open glass vials, loosely covered by Al foil to avoid dust contamination. The vials were stored in a typical chemical fume hood, with continuous air flow and vials periodically slightly tilted and rotated to expose the powder evenly to air. After these periods, the samples were transferred into an Ar filled glove box (MBraun, <0.1 ppm O_2 and H_2O) and stored inside. Another batch of as-received pristine LNMO was stored in an Ar filled glovebox for comparison, hereafter marked as LNMO_Pri.

Material characterization.—X-ray photoelectron spectroscopy (XPS) experiments were carried on two different machines at two different locations for consistency and data comparison. One set was performed on a Thermo Scientific™ Nexsa™ Surface Analysis System instrument using a monochromatic Al K X-ray source (72 W). The other set of measurements were performed on Kratos AXIS Supra+ system. Spectra were acquired using a monochromatic Al K α (1487 eV) source operating at 144 W power (12 mA \times 12 kV) and pass energies of 20 eV for high-resolution spectra and 160 eV for survey spectra. These were acquired in the hybrid spectroscopy mode over an area of approximately $700 \times 300 \mu\text{m}^2$. Charge compensation was achieved using the Kratos electron charge compensation system. Measurements were performed on powders that were fixed on a conductive carbon tape. Data acquisition was carried out using the ESCAPE software, and processing was performed with CasaXPS software (v2.3.17) utilizing a Shirley background. Peak fits were achieved using Functional Lorentzian (LF) line shapes. The peak positions were calibrated with respect to C 1s at 284.8 eV.

Scanning electron microscopy (SEM) images were recorded on a Zeiss Auriga 60 with Gemini SEM column. The pristine LNMO and the exposed samples were also analyzed by transition electron microscopy (TEM) on a double Cs aberration corrected cold FEG Jeol ARM 200FC, operated at 200 kV. Element compositions were analyzed by energy dispersive X-ray spectroscopy (EDS, 100 mm² Centurio EDS detector covering a solid angle of 0.98 Sr) and electron energy loss spectroscopy (EELS, GIF Quantum ER). EELS was performed with a dispersion of 0.25 eV channel⁻¹, giving an energy resolution of 0.8 eV. LNMO is partly beam sensitive under a 200 kV electron beam and cannot handle a too high dose of electrons per unit area. In order to avoid possible beam damage during spectroscopy mapping, the pixel time was kept at maximum

0.05 s per pixel, combined with a 110 pA beam current, a beam diameter of 0.09 nm and a pixel size of $0.10 \times 0.10 \text{ nm}^2$. The preparation of cross-sectional lamellae of the LNMO powder samples was done on a Helios G4 UX focused ion beam system. To avoid ion beam damage and implantation into the top of the sample, carbon protection layers were deposited where the initial part of the protection layer was deposited by electron beam assisted deposition. Coarse lamellae thinning was performed at 30 kV acceleration voltage for the Ga⁺ ion beam. To minimize surface damage, final thinning and polishing was done at 5 kV and then 2 kV on both sides of the lamellae.

Electrode fabrication and cell assembly.—The working electrodes for electrochemical tests were fabricated by dry grinding the LNMO powder (80 wt%) with super P carbon (SP) as conductive agent (10 wt%) and Poly tetra fluoroethylene (PTFE, powder, Sigma-Aldrich) as binder (10 wt%) for 15 min, followed by pressing the dry powder (around 3 mg) onto the coin cell case, as shown in Fig. S1. The typical active material mass loading was approximately 9 mg cm^{-2} . For the variable C-rate test, the ratio of the LNMO, SP to PTFE was 70:20:10. All the electrochemical tests were performed in half-cell configuration (CR2032, SS316 coin cell format) with a Li-metal chip as counter and pseudo-reference electrode, and one sheet of glass fiber (Whatman, GF/D) as separator. A solution of 1.2 M LiPF₆ in EC/EMC (3/7 wt./wt.) supplied by SOLVIONIC was used as electrolyte. The cells were tested in the potential range of 3.0 to 4.9 V (vs Li⁺/Li⁰) in the constant current (CC) mode (1C rate corresponding to a current of 147 mA g^{-1}). The assembly was carried out in an Ar filled glove box (MBraun, <0.1 ppm O_2 and H_2O). Galvanostatic charge-discharge tests were performed with a Neware battery testing system (BTS-4000) at ambient temperature (25 °C).

Results and Discussion

Figure 1A illustrates the protocol applied in this work for exposure of LNMO powder to ambient air, containing trace amounts of carbon dioxide (440 ppm in average) and water (75% average annual humidity), at a laboratory temperature of 19.5 °C on an annual average. These air constituents are expected to react, along with possible generated active oxygen species, at the surface of LNMO, to form primarily lithium compositions such as Li_2CO_3 , LiHCO_3 , or LiOH , along with minor Ni and Mn-based compounds. This phenomenon is in particular enhanced and documented for Ni-rich oxides while it remains an open question whether, and to what extent, it can also occur on the surface of the LNMO spinel phase, and how this can impact the electrochemical performances.^{20,21,26} To analyze these, a series of techniques have been employed to characterize the pristine LNMO and the air exposed samples, with also electrochemical properties tested, compared and evaluated to reveal the correlation.

The XPS analysis results of the pristine and 12 months aged LNMO are shown in Figs. 1B, 1C and S2. The C 1s spectra collected on both samples contain species attributed to carbonates (289 eV), C=O (288 eV), C–O (286 eV) and C–C/C–H (284.8 eV).^{27,28} A small amount of carbonates (3%) was found to exist already on the surface of pristine LNMO, most certainly formed during the sample transfer and transport processes prior to the start of the study. Little difference in the distribution of the species can be detected for both samples according to their C 1s spectra. The O 1s peaks arising from C–O, C=O/CO₃ and bulk material are located at 532.4, 531.2 and 529.7 eV, respectively, and there is no significant change after exposure to ambient air of LNMO, even for a period of 12 months (the sample aged for _2w, _2m and _6m displayed similar XPS composition and distribution, refer to Fig. S3). Similarly, the Li 1s, Mn 2p, Mn 3s and Ni 2p peaks are equal prior to and after air exposure. This suggests that storage under ambient conditions has minor influence on the surface (to a maximum depth of 5–10 nm that XPS can probe) of the LNMO

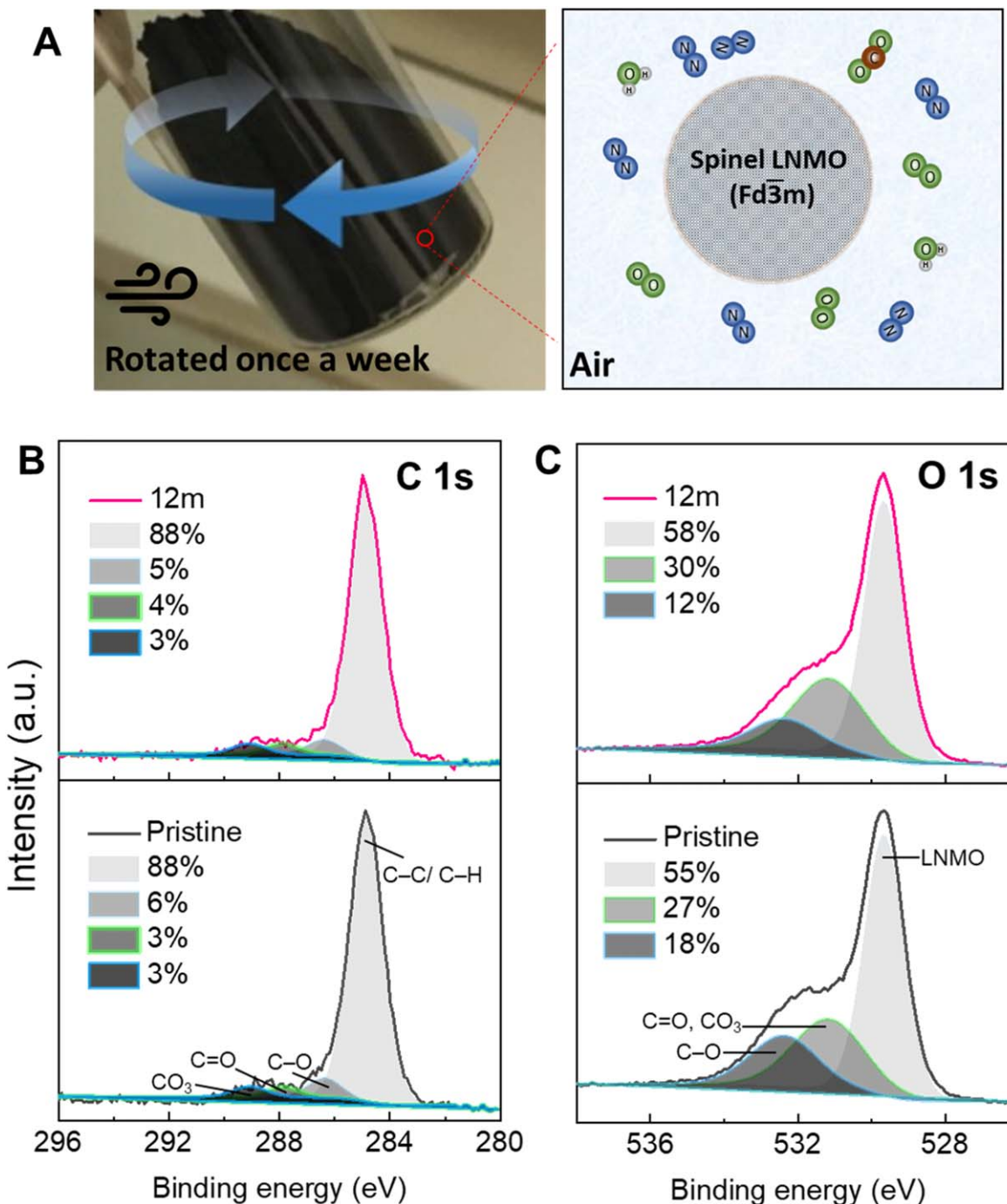


Figure 1. (A) Photograph of LNMO powder stored in the open glass vials, and exposed to ambient air conditions. The vials were periodically tilted and rotated to ensure uniform exposure. XPS spectra for the pristine sample and the sample exposed in air for 12 months: (B) C 1s and (C) O 1s signals. The atomic percentage bars and color codes are associated to the respective species.

cathode material, and that any surface changes are self-limited, and may occur shortly after the synthesis and exposure to ambient air. Additional techniques were subsequently applied to characterize the samples and understand the characteristics of this material, in particular the composition and phase evolution from outer to inner surface.

The morphology, crystal structure and elemental content of the LNMO surface were also analyzed with SEM and TEM. Bright field (BF) TEM (Figs. 2A–2B) shows that pristine LNMO particles are multi-crystalline, with faceted grain boundaries. The faceted surface morphology was also observed in SEM (inset of Fig. 2A). In the BF TEM image in Fig. 2B, the dark contrast grain is oriented on a

[1–10] zone axis. The electron diffraction pattern (inset of Fig. 2B) matches a cubic crystal with a lattice parameter of 8.1–8.2 Å. In contrast to a pure face centered unit cell, the diffraction pattern shows weak intensities in the forbidden 110 and 100 Bragg reflections. The loss of face centered ordering may be due to (partial) periodic ordering between the Mn and Ni atoms.

In the high angle annular dark field (HAADF) STEM image (Fig. 2C) the contrast scales proportionally to Z^2 (Z = atomic number) and the image shows the atomic columns containing heavy Ni/Mn elements, while atomic columns with lighter Li and/or O are not visible. In the outer few nm towards the surface, the signal increases, which is an indication of increased concentrations of Mn

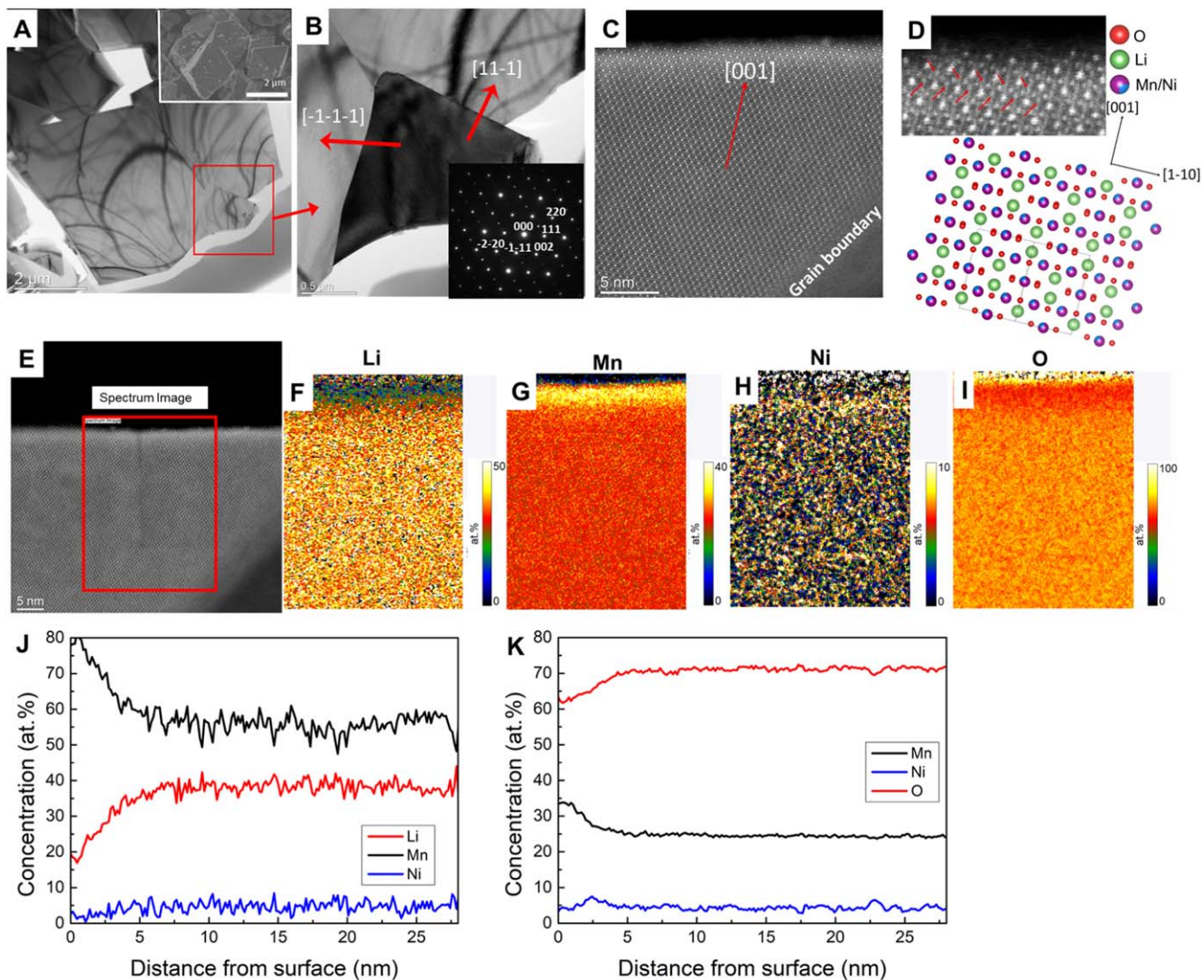


Figure 2. Characterization of pristine LNMO surface along the [001] crystallographic direction. (A) Bright field (BF) TEM image with inset of SEM image. (B) BF TEM image of a grain oriented on the [1-10] zone axis with inset of the corresponding diffraction pattern. (C) HAADF STEM image and (D) a model of the LNMO unit cell. (E) HAADF STEM image and mapping of (F) Li, (G) Mn, (H) Ni and (I) O elements with change of atom percentage in the spectrum image area by EELS. Quantitative change of the signal as a function of distance from surface by using the Li K, Mn $M_{2,3}$ and Ni $M_{2,3}$ peaks in EELS (J) and by using the O K, Mn $L_{2,3}$ and Ni $L_{2,3}$ peaks in EELS (K). In (J) the sum of Li, Mn and Ni adds up to 100% in every pixel, while in (K) the sum of Mn, Ni and O adds up to 100% in every pixel.

and/or Ni. In Fig. 2D, the surface near region from Fig. 2C is magnified and shown alongside a model of the LNMO unit cell viewed in the [110] projection. In the outer 1–2 nm, the normally invisible Li atomic columns (red arrows in Fig. 2D) show strong contrast in the dark field STEM image. This indicates that heavy transition metals are substituting Li in the outer unit cells of the material.

Elemental maps and line profiles that show the changes in the chemical composition as a function of distance from the surface are displayed in Figs. 2E–2K. The line profiles are created by averaging several tens of pixels along the horizontal direction in the elemental maps. The elemental maps and line profiles confirm the indications from the dark field STEM images that a clear increase is observed in the Mn concentration in the outer 2 nm, with a corresponding decrease of the Li concentration. Whereas the Ni concentration shows a minor increase in the 2–4 nm near-surface region, in the outer 2 nm, however, there is no observable increase in the Ni concentration. This implies that the HAADF STEM contrast at the positions of the Li atoms in the outer 2 nm are due to Mn atoms, substituting Li in this region. The O concentration is also observed to

decrease at the surface, yet this does not imply higher O vacancies in the spinel lattice at the surface. The O concentration is determined based on the relative amount of oxygen compared to Mn and Ni. Given that the Mn concentration significantly increases towards the surface, this will automatically decrease the relative concentration of O, even though the number of O atoms per unit cell is constant.

To further clarify the atomic structure and chemical composition evolution on the surface, the EEL spectra including O and Li K-peaks and Mn and Ni $L_{2,3}$ -peaks for pristine LNMO, at various distances away from the surface, are shown in Fig. 3, as well as S4 and S5. These are acquired from different surface facets to demonstrate that the findings presented and discussed in Fig. 2 are not unique to a specific surface orientation. The spectra for the surface facet of [001] are compared in Fig. 3 and taken at various distances of 0–1, 1–2, 2–3, 4–5 and 9–10 nm away from the surface to verify the evolution of the oxidation state and content of Mn.

The Mn $L_{2,3}$ peak shows a clear chemical shift towards lower onset energies towards the surface, meaning that the oxidation state is reduced (Fig. 3C). In the bulk, the oxidation state of Mn is primarily +4, with additional contribution of Mn^{3+} . On the very

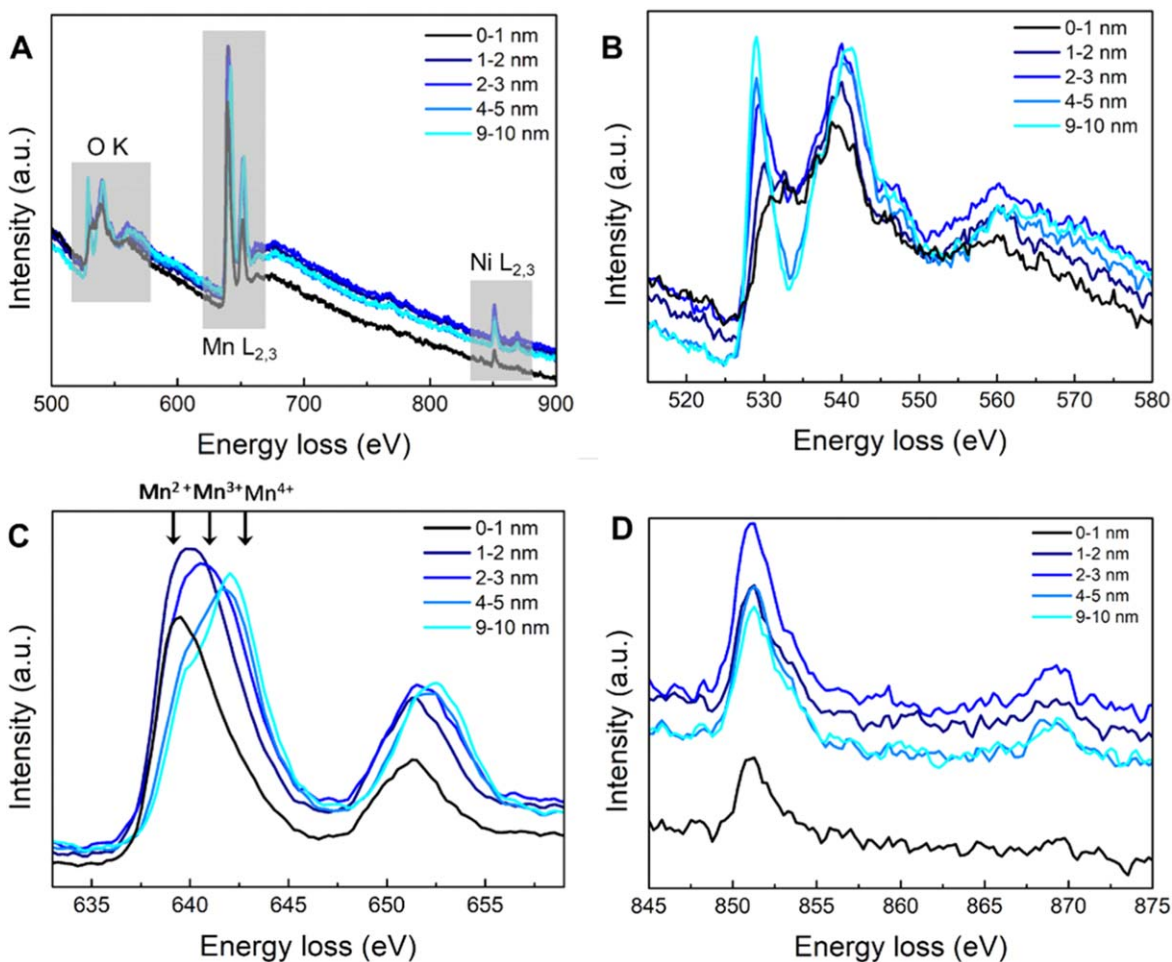


Figure 3. (A) EEL spectra collected at various distances away from the surface in the spectrum image area (Fig. 2E) of pristine LNMO, with the O K-peak and Mn and Ni $L_{2,3}$ -peaks included. The corresponding zoomed in spectra of (B) O K, (C) Mn $L_{2,3}$ and (D) Ni $L_{2,3}$.

surface, i.e., at 0–1 nm, contributions from Mn^{2+} are evident. In addition, the Li signal in outmost 1 nm is very weak, suggesting that most of the Li has been replaced by Mn, as can be seen from EEL spectra of Mn $M_{2,3}$ and Li K and corresponding atom percent values in Fig. S4. Little change can be observed for the Ni $L_{2,3}$ -peaks in Fig. 3D, indicating that the oxidation state of Ni is constant and independent of the distance to the surface. Hence deconvolution of EEL data is associated with high uncertainties, it was omitted. However, the fine structure of the oxygen signal can differ significantly for different structures. The O K-peak (Fig. 3B) shows significant changes close to the surface and transforms into a peak with a fine structure typically observed for Mn_3O_4 .²⁹ Similar analysis was also performed on the air exposed LNMO powders (Fig. S6), with no changes noted in particle morphology, crystal structure, or element distribution from surface to bulk, as compared to the pristine LNMO, implying that aging has little effect on these, and that any surface re-organization may have happened either during the synthesis, or immediately after.

It has been shown that surface structure and element distribution can have an impact on the electrochemical performance of $LiNi_{0.5}Mn_{1.5}O_4$ electrodes.¹¹ However, to the best of our knowledge, the impact on its stability under ambient storage conditions has been not specifically investigated, although it is assumed to be a stable material. According to the combined STEM-EDS-EELS analysis, it can be concluded that Mn dominates the LNMO surface, while Li and Ni tend to locate deeper into the bulk of the particles. Combined with XPS results, it can be assumed that the outermost 1–2 nm of the particles consist of a Mn_3O_4 depleted type spinel (with possible Ni substitution), given the mixed Mn valence and Li-sites occupancy.

This type of Mn_3O_4 -like structure has been reported to form on the surface of spinel $LiMn_2O_4$ and $LiNi_{0.5}Mn_{1.5}O_4$ cathode materials during electrochemical delithiation process.^{30,31} Important to highlight here is that the Mn_3O_4 like structure is already observed on the pristine material in this work, and not as a result of electrochemical delithiation. The low oxidation states of Mn on the surface can be attributed to surface loss of oxygen in the spinel phase during synthesis process, leaving oxygen deficiency sites. Mn_3O_4 is considered to have good thermodynamic stability and can be also used as photo catalyst.³² To note that photo catalytic reaction proceeds in an air-saturated and water-rich environment, confirming its enhanced stability. Thus, the generation of a stable Li-poor - Mn-rich oxide on the outer surface acts as a protecting layer, making the LNMO stable in air for long periods of time, with minimal surface structure and composition changes, and as shown next, minimal influence on electrochemical performances.

The electrochemical performances of the pristine and the ambient air exposed LNMO powder sample have been next evaluated and compared. Li half-cells have been assembled and tested to determine if the air exposure of the powders affects the electrochemical properties. To avoid interference of solvent and electrode processing (with thus additional exposure to air, moisture, or temperature treatment), a powder electrode assembly protocol was used, wherein the composite electrode was prepared by dry blending of LNMO powder, a binder (PTFE) and a conductive agent (Super P) inside a glovebox. The composite powder was then pressed onto coin cell case, and the cell assembly was finished by adding the separator, Li metal chip and the electrolyte. Figures 4A and 4B show the typical potential - capacity galvanostatic profiles for the first three cycles,

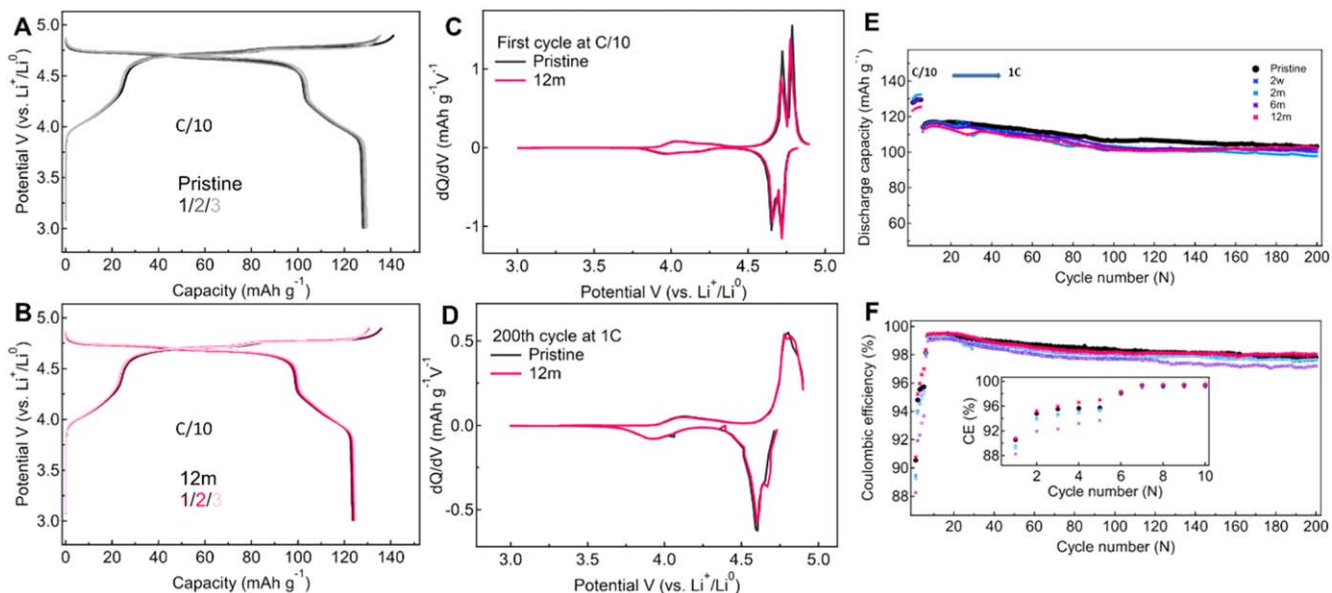


Figure 4. Galvanostatic charge-discharge potential profiles as a function of the specific capacity of the first three cycles for LNMO electrodes cycled in a lithium cell at a rate of C/10 ($1C = 147 \text{ mAh g}^{-1}$) for (A) pristine sample and (B) sample exposed for 12 months. (C) The corresponding dQ/dV differential capacity plots at the first cycle, and (D) dQ/dV plots of the 200th cycle at a rate of 1C. Cycling stability test for the pristine LNMO and all the air exposed samples: (E) specific discharge capacity and (F) coulombic efficiency vs cycle number.

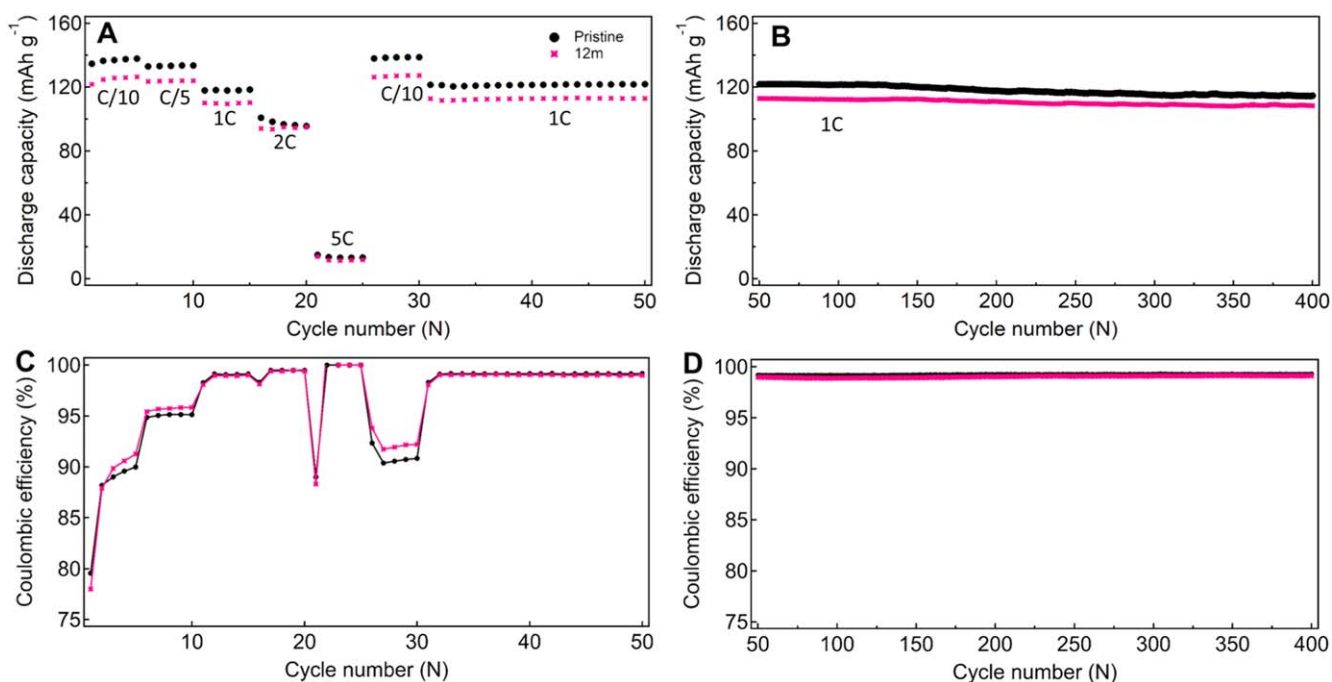


Figure 5. Power rate performance of pristine LNMO and LNMO_{12m} samples. (A) Specific discharge capacity attained for different C-rate values and (B) the long-term cycling at a rate of 1C after the C-rate test. Corresponding coulombic efficiency vs cycle number for the (C) C-rate and (D) the cycling stability test.

acquired at a rate of C/10, for pristine LNMO and LNMO_{12m} (stored under ambient conditions for 12 months). As already noted in the surface analysis section, minor differences in the galvanostatic charge-discharge profile are observed, with the LNMO_{12m} cells systematically displaying slightly lower capacity ($123 \text{ vs } 128 \text{ mAh g}^{-1}$, at the first discharge cycle). The two characteristic plateaus around 4.7 V (vs Li^+/Li) in the galvanostatic charge-discharge profiles correspond to the two sharp peaks in the differential capacity (dQ/dV) plots of both electrodes (Fig. 4C), which are related to the $\text{Ni}^{2+/\beta+}$ and $\text{Ni}^{3+/4+}$ redox couples.³³ The redox process centered around 4 V (vs Li^+/Li) is attributed to the $\text{Mn}^{3+/4+}$ couple.³⁴ The redox peaks are broadened and

slightly polarized at higher C-rate of 1C (Fig. 4D), arising from fast electron exchange, mass transfer, as well as Li-metal counter-electrode polarization with however, no significant differences noted between the two samples.

The capacity and cycling stability of the pristine and exposed (for all periods analyzed) LNMO samples are presented in Figs. 4E and 4F. Again, no significant difference in performances can be observed, with all the electrodes delivering a discharge capacity in the range of $124\text{--}133 \text{ mAh g}^{-1}$ at a rate of C/10 during the first five cycles, followed by similar gradual capacity retention attained at a rate of 1C. After 200 cycles, the capacity retention is between 98 and

103 mAh g⁻¹ for all the electrodes, with no obvious trend indicated. A similar observation can be made on the measured coulombic efficiency (CE) values, with nevertheless slightly higher CE in average for pristine samples.

Figure 5 displays the typical rate capability of the pristine LNMO and LNMO_12m electrode materials as tested in Li half-cells, under identical mass loading and cell construct (i.e. powder form electrode processing, at high mass loading). A slightly higher capacity (of about 10 mAh g⁻¹) is attained for pristine samples with the C-rate performance further found to be minimally affected by the ageing process, with proportional capacity loss upon increased C-rate for both electrodes (Fig. 5A). It should be noted that significant capacity loss at high C-rate of 5C, contradicting the intrinsic high power performances of LNMO material, is primarily due to the excessive polarization at the counter Li-metal electrode (given the high mass loading used) and thus attaining early cutoff voltage, in particular of the charge step. Both electrodes show good capacity recovery after the C-rate test, with also stable cycling at a rate of 1C (94.3% and 96.1% for pristine and LNMO_12m, respectively). Little difference can be seen in the CE values measured over the 400 cycles, the most significant being a 1.6% improvement for pristine LNMO over the LNMO_12m at the first cycle.

Conclusions

Ambient storage stability of an Al doped spinel LNMO (Li[Ni_{0.5}Mn_{1.45}Al_{0.05}]O₄) is investigated through the use of surface, bulk and electrochemical analysis techniques. Powder form samples were stored under ambient air conditions for various periods of up to 12 months and compared to the pristine LNMO. We find that the surface and bulk structure of LNMO remain minimally affected, even after a long duration of 12 months of storage. The electrochemical tests of the respective electrode materials show equally good electrochemical performances, assigned to minor surface changes after long-term air exposure, further supporting the finding of little influence of ambient storage on the electrodes. A Li depleted Mn₃O₄ type structure is detected on the outermost surface, which is at the origin of this enhanced stability. It is known that synthesis and doping can greatly affect the crystal structure and surface chemistry of LNMO. Heat treatment conditions and Al doping have been found to impact the space group of LNMO.^{35–37} Moreover, Al doping can allow LNMO to show disordered crystal structure and have higher content of Mn³⁺ in comparison to LNMO without Al doping.³⁸ Therefore, it can be assumed that the Al doping of LNMO in the current study can be at the origin of the air stability as it can cause the disordering and element substitution to form the Mn-rich layer with low valence on the surface which is more chemically stable in air. For non-doped samples, additional studies might be required, although it can be reasonably assumed that if a Li depleted Mn₃O₄ type structure is, or can be generated on the surface (either during the synthesis, or by other elements doping) similar stability properties can be expected. Overall, this study provides guidelines for, and demonstrates that the Al-doped spinel LNMO can be handled and stored under ambient conditions for long periods of time, which can simplify the storage, transportation and processing of this type of next generation cathode material.

Acknowledgments

This work was supported by EU Horizon 2020 innovation program under grant agreement number 875527—HYDRA project. DT acknowledges CSC for the PhD fellowship. JB acknowledges F.R.S-FNRS for the PhD FRiA fellowship. The authors also acknowledge the support from the Research Council of Norway to NORTEM [197405] and NorFab [245963/F50].

Data Availability

The datasets generated and analyzed in this study are available on <https://zenodo.org>.

Competing Interests

The authors declare no competing interests.

ORCID

Da Tie <https://orcid.org/0009-0000-3244-9695>
 Nils Peter Wagner <https://orcid.org/0000-0002-8014-4324>
 Raheleh Azmi <https://orcid.org/0000-0002-0000-4349>
 Killian Stokes <https://orcid.org/0000-0002-6299-1319>
 Per Erik Vullum <https://orcid.org/0000-0001-7968-4879>
 Shubhadeep Pal <https://orcid.org/0000-0001-7514-0217>
 Mihaela Buga <https://orcid.org/0000-0001-9666-2508>
 Maria Hahlin <https://orcid.org/0000-0002-5680-1216>
 Kristina Edström <https://orcid.org/0000-0003-4440-2952>
 Simon Clark <https://orcid.org/0000-0002-8758-6109>
 Alexandru Vlad <https://orcid.org/0000-0002-0059-9119>

References

- D. Deng, "Li-ion batteries: basics, progress, and challenges." *Energy Science & Engineering*, **3**, 385 (2015).
- N. Nitta, F. Wu, J. T. Lee, and G. Yushin, "Li-ion battery materials: present and future." *Mater. Today*, **18**, 252 (2015).
- W. Li, E. M. Erickson, and A. Manthiram, "High-nickel layered oxide cathodes for lithium-based automotive batteries." *Nat. Energy*, **5**, 26 (2020).
- A. Yoshino, "1 - Development of the lithium-ion battery and recent technological trends." *Lithium-Ion Batteries*, ed. G. Pistoia (Elsevier, Amsterdam) p. 1 (2014).
- D. Larcher and J. M. Tarascon, "Towards greener and more sustainable batteries for electrical energy storage." *Nat. Chem.*, **7**, 19 (2015).
- H. Wang, "LiNi_{0.5}Mn_{1.5}O₄ Cathodes for Lithium Ion Batteries: A Review." *J. Nanosci. Nanotechnol.*, **15**, 6883 (2015).
- G. Liang, V. K. Peterson, K. W. See, Z. Guo, and W. K. Pang, "Developing high-voltage spinel LiNi_{0.5}Mn_{1.5}O₄ cathodes for high-energy-density lithium-ion batteries: current achievements and future prospects." *J. Mater. Chem. A*, **8**, 15373 (2020).
- W. Li, B. Song, and A. Manthiram, "High-voltage positive electrode materials for lithium-ion batteries." *Chem. Soc. Rev.*, **46**, 3006 (2017).
- H. Xu, H. Zhang, J. Ma, G. Xu, T. Dong, J. Chen, and G. Cui, "Overcoming the challenges of 5 V Spinel LiNi_{0.5}Mn_{1.5}O₄ cathodes with solid polymer electrolytes." *ACS Energy Lett.*, **4**, 2871 (2019).
- X. Yu, W. A. Yu, and A. Manthiram, "Advances and prospects of high-voltage spinel cathodes for lithium-based batteries." *Small Methods*, **5**, e2001196 (2021).
- J. Ma, P. Hu, G. Cui, and L. Chen, "Surface and interface issues in spinel LiNi_{0.5}Mn_{1.5}O₄: insights into a potential cathode material for high energy density lithium ion batteries." *Chem. Mater.*, **28**, 3578 (2016).
- H. Wang, Z. Shi, J. Li, S. Yang, R. Ren, J. Cui, J. Xiao, and B. Zhang, "Direct carbon coating at high temperature on LiNi_{0.5}Mn_{1.5}O₄ cathode: Unexpected influence on crystal structure and electrochemical performances." *J. Power Sources*, **288**, 206 (2015).
- T. Hwang, J. K. Lee, J. Mun, and W. Choi, "Surface-modified carbon nanotube coating on high-voltage LiNi_{0.5}Mn_{1.5}O₄ cathodes for lithium ion batteries." *J. Power Sources*, **322**, 40 (2016).
- J. Chong, S. Xun, J. Zhang, X. Song, H. Xie, V. Battaglia, and R. Wang, "Li₃PO₄-coated LiNi_{0.5}Mn_{1.5}O₄: a stable high-voltage cathode material for lithium-ion batteries." *Chemistry*, **20**, 7479 (2014).
- S. Tao et al., "Nanoscale TiO₂ membrane coating spinel LiNi_{0.5}Mn_{1.5}O₄ cathode material for advanced lithium-ion batteries." *J. Alloys Compd.*, **705**, 413 (2017).
- X.-W. Gao, Y.-F. Deng, D. Wexler, G.-H. Chen, S.-L. Chou, H.-K. Liu, Z.-C. Shi, and J.-Z. Wang, "Improving the electrochemical performance of the LiNi_{0.5}Mn_{1.5}O₄ spinel by polypyrrole coating as a cathode material for the lithium-ion battery." *J. Mater. Chem. A*, **3**, 404 (2015).
- Z. Zou, H. Xu, H. Zhang, Y. Tang, and G. Cui, "Electrolyte therapy for improving the performance of LiNi_{0.5}Mn_{1.5}O₄ cathodes assembled lithium-ion batteries." *ACS Appl. Mater. Interfaces*, **12**, 21368 (2020).
- T.-F. Yi, J. Mei, and Y.-R. Zhu, "Key strategies for enhancing the cycling stability and rate capacity of LiNi_{0.5}Mn_{1.5}O₄ as high-voltage cathode materials for high power lithium-ion batteries." *J. Power Sources*, **316**, 85 (2016).
- G. Q. Liu, L. Wen, and Y. M. Liu, "Spinel LiNi_{0.5}Mn_{1.5}O₄ and its derivatives as cathodes for high-voltage Li-ion batteries." *J. Solid State Electrochem.*, **14**, 2191 (2010).
- J. Sicklinger, M. Metzger, H. Beyer, D. Pritzl, and H. A. Gasteiger, "Ambient storage derived surface contamination of NCM811 and NCM111: performance implications and mitigation strategies." *J. Electrochem. Soc.*, **166**, A2322 (2019).
- R. Jung, R. Morasch, P. Karayaylali, K. Phillips, F. Maglia, C. Stinner, Y. Shao-Horn, and H. A. Gasteiger, "Effect of ambient storage on the degradation of ni-rich positive electrode materials (NMC811) for Li-Ion batteries." *J. Electrochem. Soc.*, **165**, A132 (2018).
- C. Lv, Z. Li, X. Ren, K. Li, J. Ma, and X. Duan, "Revealing the degradation mechanism of Ni-rich cathode materials after ambient storage and related regeneration method." *J. Mater. Chem. A*, **9**, 3995 (2021).
- Q. Xie and A. Manthiram, "Long-life, ultrahigh-nickel cathodes with excellent air storage stability for high-energy density lithium-based batteries." *Chem. Mater.*, **32**, 7413 (2020).

24. C. Busà, M. Belekoukia, and M. J. Loveridge, "The effects of ambient storage conditions on the structural and electrochemical properties of NMC-811 cathodes for Li-ion batteries." *Electrochim. Acta*, **366** (2021).
25. P. Oh, B. Song, W. Li, and A. Manthiram, "Overcoming the chemical instability on exposure to air of Ni-rich layered oxide cathodes by coating with spinel LiMn_{1.9}Al_{0.1}O₄." *J. Mater. Chem. A*, **4**, 5839 (2016).
26. C. Wang, L. Shao, X. Guo, X. Xi, L. Yang, C. Huang, C. Zhou, H. Zhao, D. Yin, and Z. Wang, "Air-induced degradation and electrochemical regeneration for the performance of layered Ni-rich cathodes." *ACS Appl. Mater. Interfaces*, **11**, 44036 (2019).
27. R. A. Quinlan, Y.-C. Lu, D. Kwabi, Y. Shao-Horn, and A. N. Mansour, "XPS Investigation of the electrolyte induced stabilization of LiCoO₂ and 'AlPO₄'-coated LiCoO₂ composite electrodes." *J. Electrochem. Soc.*, **163**, A300 (2015).
28. Y. You, H. Celio, J. Li, A. Dolocan, and A. Manthiram, "Modified high-nickel cathodes with stable surface chemistry against ambient air for lithium-ion batteries." *Angew. Chem.*, **130**, 6590 (2018).
29. L. Laffont and P. Gibot, "High resolution electron energy loss spectroscopy of manganese oxides: application to Mn₃O₄ nanoparticles." *Mater. Charact.*, **61**, 1268 (2010).
30. D. Tang, Y. Sun, Z. Yang, L. Ben, L. Gu, and X. Huang, "Surface structure evolution of LiMn₂O₄ cathode material upon charge/discharge." *Chem. Mater.*, **26**, 3535 (2014).
31. M. Lin et al., "Insight into the atomic structure of high-voltage Spinel LiNi_{0.5}Mn_{1.5}O₄ cathode material in the first cycle." *Chem. Mater.*, **27**, 292 (2014).
32. A. Sukhdev, M. Challa, L. Narayani, A. S. Manjunatha, P. R. Deepthi, J. V. Angadi, P. Mohan Kumar, and M. Pasha, "Synthesis, phase transformation, and morphology of hausmannite Mn(3)O(4) nanoparticles: photocatalytic and antibacterial investigations." *Heliyon*, **6**, e03245 (2020).
33. R. Qiao, L. A. Wray, J.-H. Kim, N. P. W. Pieczonka, S. J. Harris, and W. Yang, "Direct experimental probe of the Ni(II)/Ni(III)/Ni(IV) Redox Evolution in LiNi_{0.5}Mn_{1.5}O₄ electrodes." *The Journal of Physical Chemistry C*, **119**, 27228 (2015).
34. Y. Xiao, J. Fan, X. Zhang, D. Zhang, and C. Chang, "Li₂Ni_{0.5}Mn_{1.5}O₄, spinel type cathode material with high reversible capacity." *Electrochim. Acta*, **311**, 170 (2019).
35. G. Ganas, G. Kastrinaki, D. Zarvalis, G. Karagiannakis, A. G. Konstandopoulos, D. Versaci, and S. Bodoardo, "Synthesis and characterization of LNMO cathode materials for lithium-ion batteries." *Mater. Today Proc.*, **5**, 27416 (2018).
36. G. B. Zhong, Y. Y. Wang, X. J. Zhao, Q. S. Wang, Y. Yu, and C. H. Chen, "Structural, electrochemical and thermal stability investigations on LiNi_{0.5}-xAl_{2x}Mn_{1.5}-xO₄ (0 ≤ 2x ≤ 1.0) as 5 V cathode materials." *J. Power Sources*, **216**, 368 (2012).
37. P. Sun, Y. Ma, T. Zhai, and H. Li, "High performance LiNi_{0.5}Mn_{1.5}O₄ cathode by Al-coating and Al³⁺-doping through a physical vapor deposition method." *Electrochim. Acta*, **191**, 237 (2016).
38. Y. Luo, T. Lu, Y. Zhang, L. Yan, S. S. Mao, and J. Xie, "Surface-segregated, high-voltage spinel lithium-ion battery cathode material LiNi_{0.5}Mn_{1.5}O₄ cathodes by aluminium doping with improved high-rate cyclability." *J. Alloys Compd.*, **703**, 289 (2017).